The Geological Society of America
Special Paper 542

Cyclostratigraphic investigations in the Calcare Massiccio (Early Jurassic, Umbria-Marche Basin) through photogrammetry

Luca Penasa
Department of Geosciences, Università degli Studi di Padova, via Gradenigo, 6, 35135 Padova, Italy, and
Center of Studies and Activities for Space (CISAS), "G. Colombo" Università degli Studi di Padova, via Venezia 15, 35131 Padova, Italy

Marco Franceschi*
Department of Geosciences, Università degli Studi di Padova, via Gradenigo, 6, 35135 Padova, Italy

Giovanni Gattolin
Department of Geosciences, Università degli Studi di Padova, via Gradenigo, 6, 35135 Padova, Italy, and
Upstream and Technical Services, Eni S.p.A., via Emilia 1, 20097, San Donato Milanese, Italy

Nereo Preto
Department of Geosciences, Università degli Studi di Padova, via Gradenigo, 6, 35135 Padova, Italy

Marc-Pierrot Deseilligny
École Nationale des Sciences Géographiques, 6-8 Avenue Blaise Pascal, Cité Descartes, Champs-sur-Marne, Marne la Vallée 77455, France

Alessandro Montanari
Osservatorio Geologico di Coldigioco, Contrada Coldigioco 4, 62021 Apiro, Italy

ABSTRACT

In this paper, we present a case study to demonstrate the potential of photogrammetry in cyclostratigraphic applications. To this end, we considered an ~300-m-thick section exposing the Lower Jurassic Calcare Massiccio Formation in the Marche Apennines of central Italy. The Calcare Massiccio comprises a thick succession of peritidal shallow-water carbonates displaying a prominent sedimentary cyclicity, where supratidal and subtidal facies alternate. The section investigated in this study is exposed on the wall of an active quarry and is almost completely inaccessible because it is vertical and because of safety and liability regulations. This setting prevents the application of standard sampling and facies analysis techniques on the whole series. An accurate three-dimensional model of the quarry wall was therefore produced by processing ~360 digital images through photogrammetry

*e-mail: marco.franceschi@unipd.it

Penasa, L., Franceschi, M., Gattolin, G., Preto, N., Deseilligny, M.-P., and Montanari, A., 2019, Cyclostratigraphic investigations in the Calcare Massiccio (Early Jurassic, Umbria-Marche Basin) through photogrammetry, *in* Koeberl, C., and Bice, D.M., eds., 250 Million Years of Earth History in Central Italy: Celebrating 25 Years of the Geological Observatory of Coldigioco: Geological Society of America Special Paper 542, p. 87–103, https://doi.org/10.1130/2019.2542(04).

and generating a high-resolution (centimeter-scale) point cloud of the outcrop with red-green-blue (RGB) values associated with each point. An ~150-m-long log representing color variations on a continuous portion of the exposed succession was then extracted from the point cloud by converting the original RGB values to grayscale values. The main facies were directly investigated in an ~10-m-long accessible section that was logged and sampled, and it was established that supratidal facies with planar stromatolites and teepee structures are darker in color, while subtidal facies, made of bioturbated mudstones to floatstones with gastropods and oncoids, display lighter color. This provided ground-truth data with which to interpret the grayscale variations in terms of facies alternations. Time-series analysis was then carried out on the grayscale series, and this revealed prominent cyclicities. Because the biochronostratigraphic framework of the Calcare Massiccio is poor, the potential orbital origin of these frequencies was tested with the average spectral misfit technique. Preliminary results suggest that the observed spectral features are compatible with Milankovitch periods and that astronomical forcing might have been a major driver in the deposition of the Calcare Massiccio Formation. Furthermore, they testify to the great potential of photogrammetry in cyclostratigraphic applications, especially when large-scale, inaccessible outcrops have to be investigated.

INTRODUCTION

Remote sensing has been used to provide lithological information by imaging outcrops of sedimentary rocks (e.g., Burton et al., 2011; Franceschi et al., 2009; Kern et al., 2013; Kurz et al., 2012; Penasa et al., 2014). The application of this method to the study of outcrops (McCaffrey et al., 2005; Trinks et al., 2005; Buckley et al., 2013; Hodgetts, 2013; Buckley et al., 2008) has two principal strengths: (1) It makes it possible to retrieve information from exposures that are too large and/or too difficult to access for hand-logging or sampling; and (2) it provides large amounts of data in a short time.

Furthermore, remote-sensing techniques have the potential to quantify the high-resolution lithological variability throughout long stratigraphic series, and this makes them of interest for cyclostratigraphy. Examples of the applications of visible cameras for retrieving cyclostratigraphic data from outcrops can be found in Schwarzacher (1993), Zeeden et al. (2015, 2016), and Cozzi et al. (2005). One of the main issues when working with cameras, however, is finding suitable points of view to minimize the need of perspective correction of the photos and avoid distortions that may hamper cyclostratigraphic interpretation.

Three-dimensional (3-D) imaging of outcrops with terrestrial laser scanners (TLSs) can overcome these issues (Franceschi et al., 2009), and it has been successfully applied to cyclostratigraphy (Franceschi et al., 2011, 2015). Although TLS devices provide long-range, high-resolution acquisition and do not have the problem of perspective distortion, they have the disadvantage of being sometimes difficult to transport, especially in operative conditions that require long walks or positioning of the instrument on difficult terrain.

In photogrammetry, a 3-D reconstruction of objects is performed starting from 2-D images taken with cameras, provided that these images are taken from properly located points of view (Westoby et al., 2012). Photogrammetry couples the portability and flexibility of camera systems, which far exceeds that of laser scanners, and their capability of retrieving quantitative lithological information, and so it represents a potentially interesting data-acquisition option for cyclostratigraphy in some operational contexts. In this chapter, we present a case history where photogrammetric imaging was applied to the cyclostratigraphic investigation of a peritidal carbonate platform unit in the Lower Jurassic Calcare Massiccio Formation, central Italy.

The Calcare Massiccio Formation encompasses a thick succession (in this area, typically 700–800 m) of shallow-water carbonates that display a prominent sedimentary cyclicity (Petti et al., 2007). However, the thickness of the formation and the conditions of the outcrops, often exposed on vertical and thus inaccessible walls, have so far made cyclostratigraphic investigations difficult.

The realization of a photogrammetric model of the wall of a large active quarry in the Calcare Massiccio permitted us to quantify color variations in the form of grayscale series covering a long stretch of the exposed stratigraphic interval. Changes in color were linked to facies variations through direct observation on an accessible portion of the series, and then grayscale series were analyzed through signal processing methods to highlight possible orbital cyclicities.

To the best of our knowledge, this represents the first attempt to provide a cyclostratigraphic characterization of the Calcare Massiccio by means of remote sensing and the first time that photogrammetry has been applied to cyclostratigraphy. The outcome of this contribution is therefore twofold. On the one hand, the potential of a relatively fast and low-cost technique in retrieving cyclostratigraphic data from large outcrops is demonstrated, and on the other hand, results of the cyclostratigraphic analysis

provide insights on the possible orbital control on the cyclical organization of the Calcare Massiccio.

GEOLOGIC SETTING

The Gola Della Rossa quarry is located near the town of Serra San Quirico, 45 km west of the port city of Ancona in the Marche region of central Italy, and it offers a spectacular exposure of the Calcare Massiccio (Fig. 1). The Calcare Massiccio is a stratigraphic unit of the Umbria-Marche sedimentary succession that was deposited on the passive margin of the Adria microplate beginning at the end of the Triassic, and it is now exposed on the fold-and-thrust mountain belt of the northeastern Apennines. The Umbria-Marche stratigraphic succession starts with an Upper Triassic transgression on top of Hercynian crust (Santantonio et al., 1996), followed by deposition of the evaporitic deposits of the Burano Formation (Lugli, 2001; Martinis and Pieri, 1964). The Calcare Massiccio was then deposited during a time span ranging from the Hettangian to the Sinemurian, and it represents the onset of a tropical shallow-water carbonate platform characterized by peritidal cyclicity mainly organized in shallowing-upward cycles (Brandano et al., 2015; Colacicchi et al., 1975). The thickness of the Calcare Massiccio increases from some hundreds of meters in the Latium-Abruzzi platform to a typical thickness of 500–700 m in the Umbria-Marche region (Carminati et al., 2013). However, at Monte Murano, where the Gola Della Rossa quarry is located, the Calcare Massiccio exhibits a thickness exceeding 700 m (Fig. 2). The Calcare Massiccio carbonate platform underwent

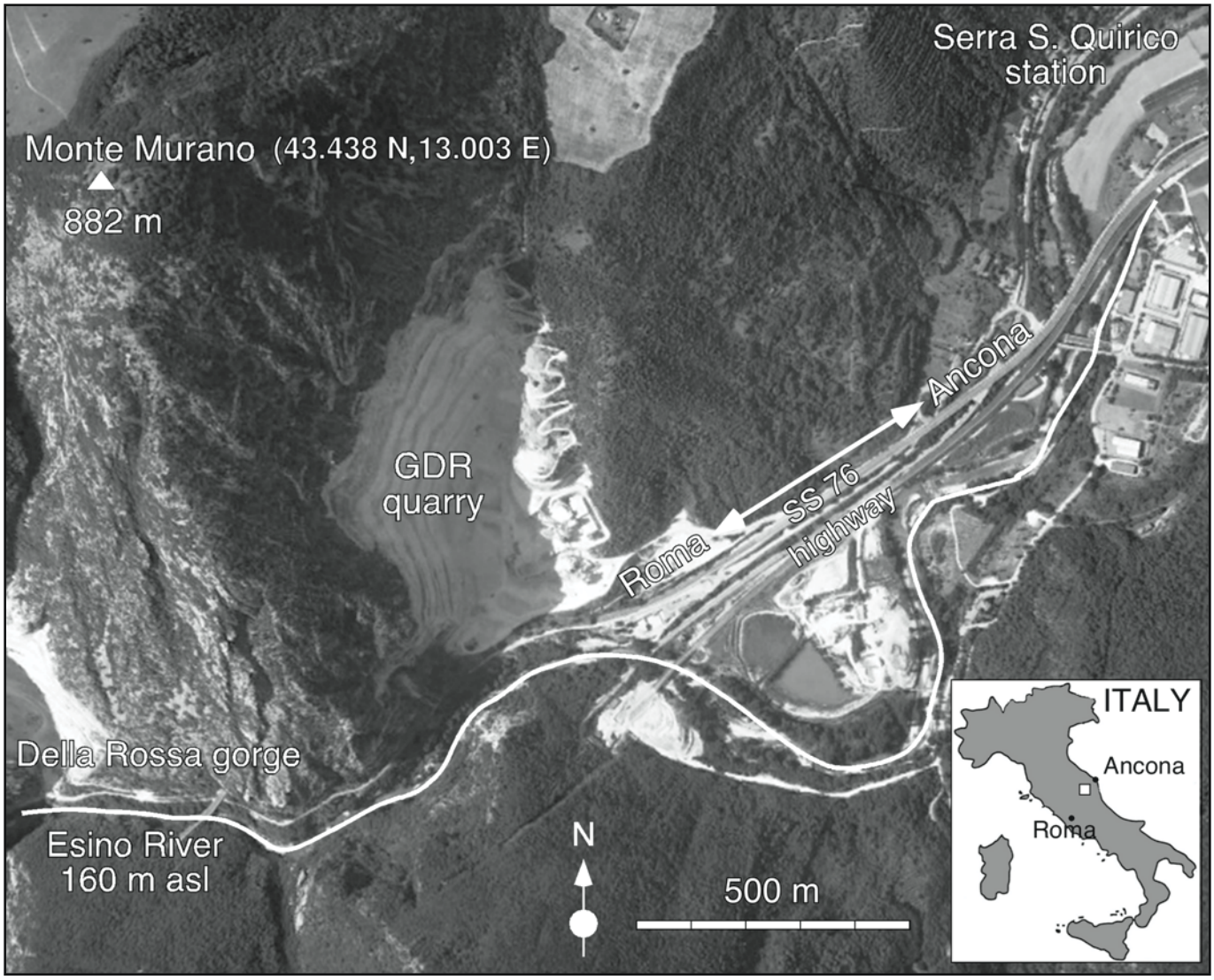

Figure 1. Google Earth map of the Gola Della Rossa quarry (GDR), located in central Italy, near the town of Serra San Quirico, Ancona Province, Italy (asl—above sea level).

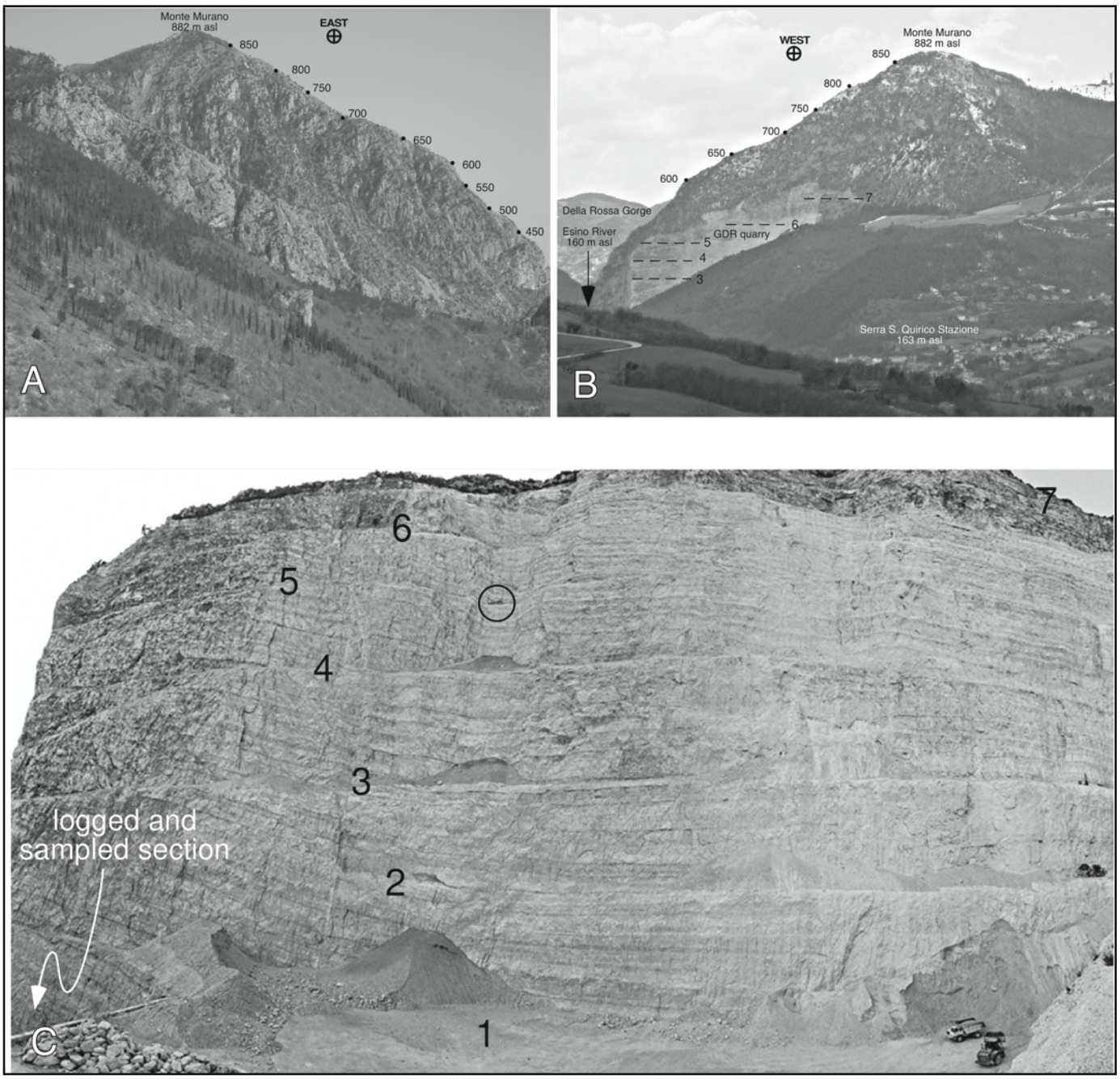

Figure 2. (A–B) Photos of Calcare Massiccio continuously exposed at Monte Murano as seen from (A) the west and (B) the east. Elevations were taken from a detailed topographic map (asl—above sea level). In the panoramic view of the eastern side of the mountain, the benches on the main Gola Della Rossa quarry (GDR) face are shown and numbered. (C) Wide-angle view of the quarry front, ~300 m high and 500 m wide. Circle indicates a caterpillar bulldozer working on the fifth bench.

tectonic fragmentation and subsequent localized and progressive drowning during the Sinemurian (Marino and Santantonio, 2010; Bice and Stewart, 1985, and references therein), creating an architecture of scattered structural highs surrounded by deep-water pelagic basins (Coltorti and Bosellini, 1980). The Calcare Massiccio displays a prominent cyclicity that was interpreted as potentially related to Milankovitch cycles by Brandano et al. (2015), who performed time-series analysis of a 26-m-long facies-thickness rank series retrieved in a section outcropping in the Cornicolani Mountains (some 100 km SSW from Gola Della Rossa), encompassing a relatively short stratigraphic interval just below the drowning of the platform. The outcrop under

TABLE 1. DESCRIPTION OF FACIES IDENTIFIED IN THE 10-M-LONG SECTION FROM GOLA DELLA ROSSA QUARRY, AND INTERPRETATION OF THE SEDIMENTARY ENVIRONMENTS

Facies code	Facies	Description	Interpretation
1	Gastropod lime mudstone	Bioturbated lime mudstone with bivalves, gastropods, and rare foraminifera, in meter-scale beds. Irregular, centimeter-scale cavities open in the lime mud matrix.	Low-energy subtidal
2	Fenestral lime mudstone	Meter-scale beds of lime mudstone with clotted peloidal fabric and irregular and planar fenestrae, with *Thaumatoporella* sp., rare bivalves, and gastropods.	Layered thrombolite, subtidal?
3	Oncoidal rudstone	Centimeter- to decimeter-scale lenses of oncoid and intraclast rudstone with irregular base, closing laterally in a few meters, and intercalated with bioclastic wackestone to packstone. Worn gastropods and *Cayeuxia* sp. are common. Intraclasts have clotted peloidal fabric.	High-energy subtidal
4	Grainstone-rudstone with pisoids	Decimeter- to meter-scale beds of grainstone-rudstone with pisoids and oncoids, planar fenestrae, and tepee structures. Large cavities within tepees have geopetal infillings with oncoids, pisoids, and gastropods. All grains are bound by laminated microbialites with clotted peloidal fabric with planar fenestrae.	Supratidal

investigation is the front of an active quarry on the eastern slope of Monte Murano (43°26′13.54″N, 13°00′08.12″E; 886 m above sea level), and it displays a series of seven staircased access roads on benches reaching the quarrying front (~500 m wide and >300 m high) separated by vertical walls (Fig. 2C). Due to safety and liability issues, it is not possible to reach the wall, and access for this study was granted for two days during a weekend for producing a set of pictures used for the photogrammetric reconstruction (Fig. 2C).

FACIES ANALYSIS

Although the studied outcrop was almost completely inaccessible, it was possible to reach a short, ~10-m-thick section at the base of the quarry walls. This was logged in detail, and 16 samples were collected and prepared as petrographic thin sections.

Four main facies were identified on the basis of field observations and microfacies analysis (Table 1), which represent marine shallow-water depositional environments on a carbonate platform with mostly high hydrodynamic energy levels (with the sole possible exception of facies 1). Carbonate precipitation is attributed mainly to microbial processes, in the form of bed-shaped stromatolites and thrombolites, and minor calcimicrobes.

These four facies are organized in meter-scale, asymmetric, shallowing-upward peritidal cycles. Two of these cycles are encompassed by the measured section.

In the field, facies appear to have colors varying from white to dark brownish gray. The reason for color variations was investigated by identifying the mineralogical components of the facies on the 16 available thin sections (Table 2).

Petrographic observations indicate that all dark samples contain pyrite, while light-gray to white samples do not. It is thus inferred that the dark color of some layers results from the presence of pyrite. Pyrite occurs either as large (>10 µm) framboids or, more commonly, crystals with a square section. In a few samples, pyrite is concentrated near or within calcite-filled veins.

A less strict association exists between dark colors and microbialitic fabrics, and specifically stromatolitic fabrics. Supratidal facies are more likely to be dark. There might thus be a genetic association between the precipitation of diagenetic pyrite and microbialites. We hypothesize that pyrite precipitated within microbial mats in the shallow subsurface, where oxygen was consumed by the respiration of dead microbial organic matter by heterotrophic bacteria, as also commonly occurs in recent marine microbial mats (Dupraz et al., 2009).

PHOTOGRAMMETRIC SURVEY

The photogrammetric reconstruction of the virtual outcrop model (VOM) of the Gola della Rossa quarry was carried out using the open-source software suite MicMac (Rupnik et al., 2017). The MicMac[1] software package provides a complete suite of tools for performing photogrammetric reconstruction based on structure from motion (SfM) methods. Pictures of the quarry walls were taken from different viewpoints and were processed to produce a 3-D representation of the outcrop in the form of a point cloud. Each point in the point cloud has 3-D coordinates and an associated red-green-blue (RGB) value, which was obtained from the pictures themselves.

Images were acquired in RAW format using a SONY A200 DLSR digital camera at 10.20 megapixel resolution (3872 × 2600). This camera was equipped with a 28 mm lens (equivalent to ~42 mm on full frame sensors), corresponding to a field of view of 30°. This choice made it possible to obtain pictures including large portions of the quarry walls while having 10 cm pixel size at an average distance of 200 m.

Images were acquired from multiple, scattered positions (more than 10) at a distance from the outcrop ranging from 100 to 250 m. For each position, we collected enough images to

[1]https://micmac.ensg.eu/

TABLE 2. CORRESPONDENCE OF SAMPLE COLOR WITH THE OCCURRENCE OF PYRITE AND STROMATOLITIC FABRIC IN THE 16 ANALYZED THIN SECTIONS

Sample	Color	Facies code	Stromatolitic fabric	Oxidized pyrite
GDR 01	Light	1		
GDR 02	Light	1		
GDR 03	**Dark**	3	**Yes**	Yes
GDR 04	Light	1		
GDR 05	Light	3		
GDR 06	**Dark**	3		Yes
GDR 07	**Dark**	4	**Yes**	**Yes**
GDR 08	Light	2	Yes (irregular)	
GDR 09	Light	1		
GDR 10	Light	2	**Yes**	
GDR 10	**Dark**	3	**Yes**	**Yes**
GDR 11	Light	1		
GDR 12	**Dark**	4	**Yes**	Yes (scarce)
GDR 13	Light	4		
GDR 14	Light	4	**Yes**	
GDR 15	**Dark**	4	**Yes**	**Yes**
GDR 15	Light	4	**Yes**	
GDR 16	Light	3		Yes (scarce)

Note: Some samples were collected at the boundary between two facies or colors, and are thus here described as separate items.

cover the visible outcrop surface. The whole set of pictures was acquired in 1 day of fieldwork, and it was composed of ~360 images, which were then employed for photogrammetric reconstruction using MicMac.

MicMac enables the user to obtain detailed control of the various phases of the reconstruction. This aspect was of primary importance to exclude artifacts in the color information that was associated with each point of the point cloud, which may not be controlled by using commercial software. The photogrammetric reconstruction can be summarized in two steps:

(1) Camera calibration and bundle adjustment. In this step, all the internal parameters of the camera are determined (including the lens focal length and other optical parameters), together with the external parameters for each image (camera location at shoot time and its orientation in space with respect to the other frames). This is accomplished by using the Tapioca and Tapas tools of MicMac. The Tapioca tool extracts a set of key points from each picture, while Tapas uses the key points to determine the parameters and generate a low-resolution sparse point cloud. Camera positions are obtained by choosing one of the images in the data set and assigning to it a fixed position and orientation in space. All the other pictures are then added in an iterative error-minimization process until the position and orientation of all the cameras are finally known. We obtained an average pixel reprojection error lower than one pixel for all the images, and >98% of key points were retained, for a total number of >1 million key points, confirming that the poses of all >300 camera locations were faithfully estimated.

(2) Dense point cloud generation. From the whole set of images, 12 were selected to be used as master images during the dense point cloud reconstruction. MicMac requires the user to select specific images that will undergo a dense-matching process: for each pixel of the master image, a point in the 3-D space is computed. Thanks to this one-to-one correspondence between the pixels and points of the cloud, the color information embedded in the image is transferred directly to the point cloud without the need of additional processing (e.g., interpolations).

Although ~360 images were acquired, these were used only in step 1, for providing accurate and reliable camera intrinsic and extrinsic parameter determination. When step 2 was performed, MicMac automatically selected a smaller subset (typically 3–5 images) useful for reconstructing the specific master image. At the end of this process, we obtained 12 point clouds, each containing the color information derived from the corresponding master image, each of which had between 5×10^6 and 10×10^6 points.

The 12 master images, from which the point clouds were computed, were selected to be part of a set of pictures that were taken closely in time while still representing different portions of the quarry, possibly taken from a frontal position with respect to the outcrop. This selection was made to ensure that all the pictures would have been taken under similar illumination conditions, ensuring consistent color representation. Note that the 3-D reconstruction algorithm can account for changes in the illumination conditions or color rendition without limiting the dense

matching process; however, it is necessary to have the same lighting conditions in the master images if a reliable analysis of color changes is to be undertaken.

For scaling purposes, two partially overlapping point clouds obtained with an Optech ILRIS 3-D TLS were also acquired. Due to the small field-of-view of the device (40° with square-shaped footprint), only a small portion of ~150 × 170 m was covered by each scan.

The two TLS-derived point clouds, which provide a real metric framework, were coregistered using the software CloudCompare (Girardeau-Montaut, 2014): several homologous points were identified on each cloud and used to merge them into an unique point cloud through a rigid transformation and then used as a scale reference (Fig. 3A). The final scale factor for the photogrammetric point clouds was determined by performing a "fine-registration" of the TLS cloud with the corresponding portion of the photogrammetric model, using a modified iterative closest point (ICP) algorithm, as described by Zinßer et al. (2005). The final registration root mean square error (RMS) was below 25 cm.

GRAYSCALE SERIES GENERATION

The point clouds were processed in order to obtain three time series, representing grayscale variations along the stratigraphic sequence. For this, the RGB information associated with each point was converted into a grayscale value by averaging the values of the three channels. The data reduction, which

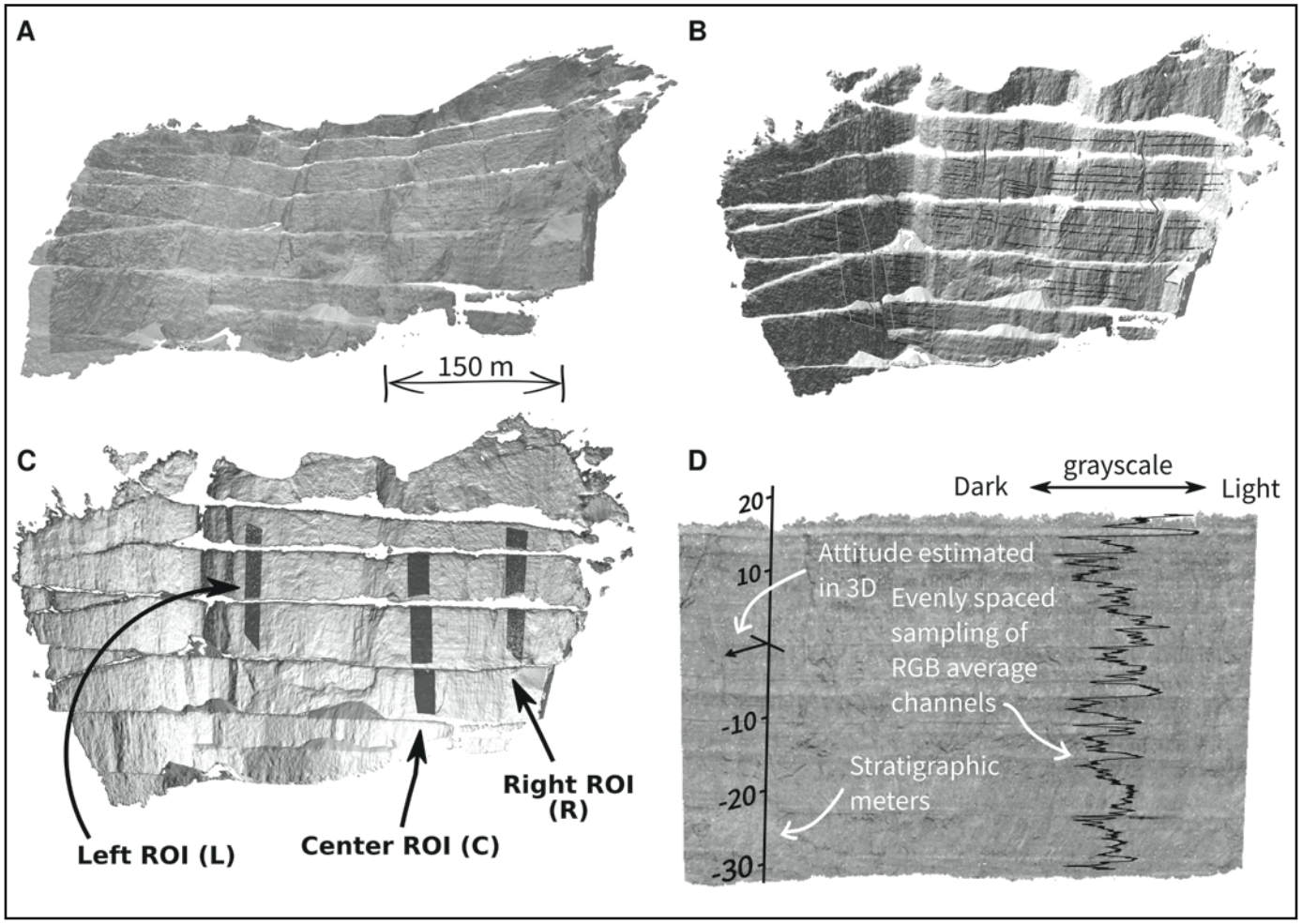

Figure 3. Phases of time-series generation starting from point clouds obtained from the photogrammetric reconstruction. (A) Point clouds were generated using the MicMac suite of software tools. (B) Linear features (layers and faults) were traced on the three-dimensional (3-D) model using CloudCompare software and helped to identify areas most suitable for further analysis. (C) Smaller regions or regions of interest (ROIs) were identified on the point clouds to be used for the time-series reconstruction. (D) Vombat plugin was used to compute evenly spaced time series of the average red-green-blue (RGB) colors perpendicular to bedding, producing grayscale logs of the sequence.

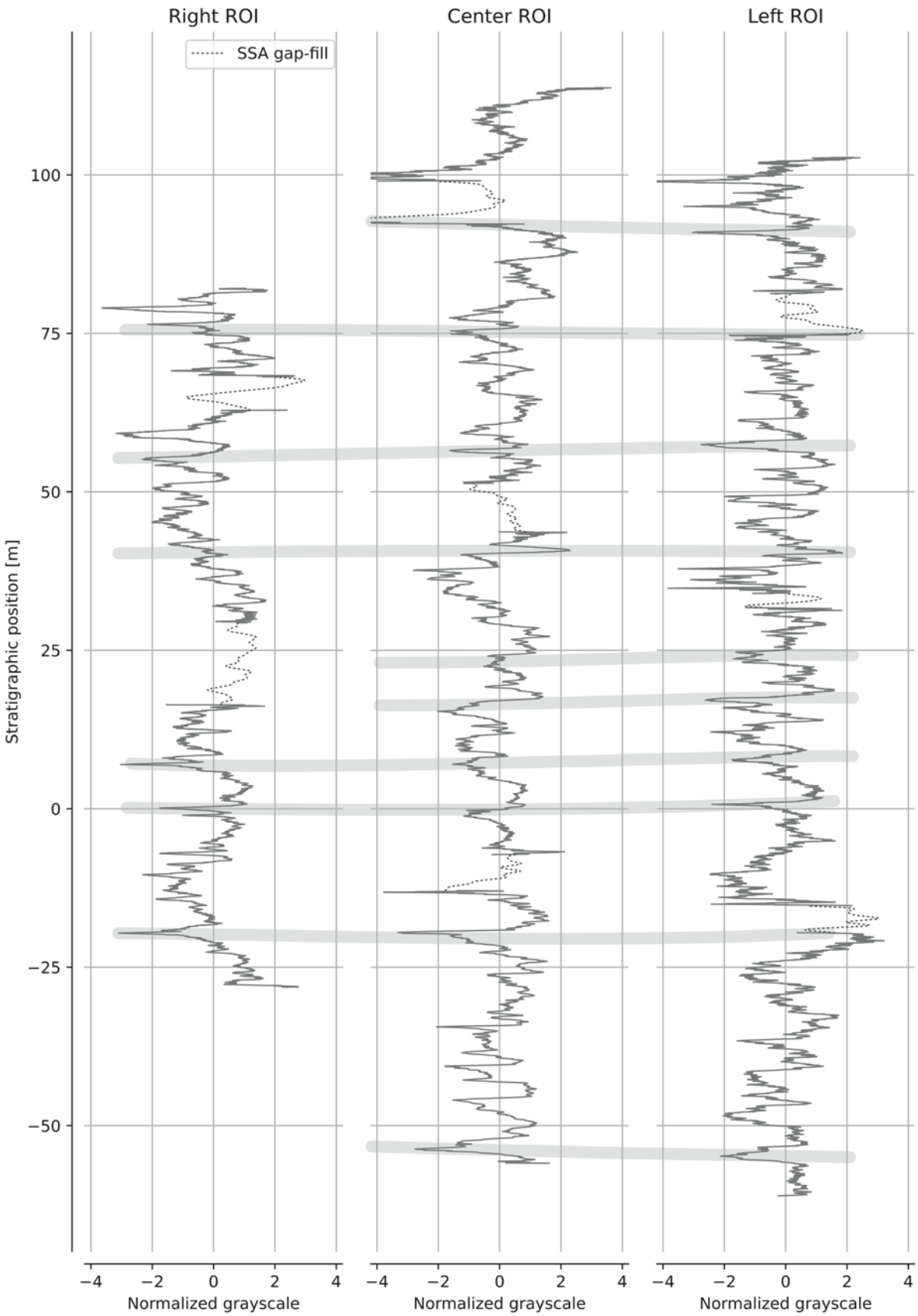

Figure 4. Three time series obtained from the right (R), center (C), and left (L) regions of interest (ROIs). Missing portions due to occluded views in the images were filled with singular spectrum analysis (SSA) gap-filling technique.

produces a one-dimensional (1-D) continuous stratigraphic log from 3-D information, was performed using the Vombat plugin[2] for CloudCompare.

The following steps were employed to produce three grayscale stratigraphic logs:

(1) All major bedding planes and faults were mapped directly on the 3-D model as polylines, to provide a basic interpretative framework (Fig. 3B).
(2) Three undisturbed regions of interest (ROIs) were identified (R, C, and L in Fig. 3C) that could be representative of overlapping stratigraphic intervals. The three regions were selected in order to maximize the total stratigraphic thickness.
(3) The average bedding attitude for each of the selected ROIs was estimated. Vombat computes the best-fitting attitude by considering multiple linear traces of the bedding planes (Fig. 3B).
(4) For each ROI, a unique attitude was used to identify a 3-D "stratigraphic reference frame," which is basically a virtual ruler perpendicular to the bedding and oriented with the positive "time" direction of the sedimentary sequence (Fig. 3D).
(5) To create a common reference frame for all three ROIs and the respective stratigraphic reference frames, we identified the same stratigraphic horizon in each ROI, on which we placed the stratigraphic zero. The alignment of the stratigraphic reference frames was then made automatically by the software on the basis of an error minimization procedure, by "sliding" the three virtual rulers in order to accommodate the imposed constraints.

A time series representative of the grayscale variations along the stratigraphic sections was generated for each ROI as a weighted running average of the grayscale values associated with the points, using Vombat. The running average for the three ROIs was performed with a 2 cm sampling step and a Gaussian kernel bandwidth (window dimension) of the same size. The sampling step controlled the final number of samples, while the bandwidth determined the "smoothness" of the generated time series.

The grayscale values in the series do not strictly correspond to the colorimetric properties of the rock, which could be measured only under controlled conditions and would require color calibration (Kirillova and Sileva, 2017). For this reason, the three grayscale logs were normalized and detrended with a third-order polynomial (Fig. 4), making them more comparable.

The three final time series are between 100 m and 150 m long with a 2 cm resolution, but they also display gaps (ranging in thickness from 5 to 10 m) corresponding to missing portions of the 3-D models, which were caused by occluded views. Gaps were filled with the SSA (singular spectrum analysis) gap-filling technique (Kondrashov and Ghil, 2006). This method first decomposes the available signal into its principal components (i.e., by performing singular spectrum analysis) and then uses those components that account for the majority of the variance to complete the missing portions with a signal that exhibits the same spatial variability present in the original data set.

In order to provide a single time series spanning the largest possible stratigraphic interval, portions of the L and C logs were used to produce a composite time series (Figs. 3 and 4) by merging uninterrupted intervals into an single log.

RESULTS

Spectral Analysis

Figure 5 shows an extract of the left ROI time series from 45 to 74 m. The series is characterized by the presence of a set of prominent dark levels (i.e., lower grayscale value; see arrows in Fig. 5) describing a cyclic pattern with a period of ~5–6 m. The darker levels are followed by an abrupt increase in grayscale value that then progressively decreases until it reaches the next minimum, sometimes passing through a series of minor oscillations of the order of 1 m in a period. This pattern occurs commonly in the extracted time series, and it could be interpreted as reflecting the typical asymmetric nature of peritidal depositional cycles (e.g., Fischer, 1964), in which supratidal facies (darker in color and therefore corresponding to the narrow minima in the grayscale time series) alternate with subtidal facies, which can be associated to lighter colors.

The three grayscale series were investigated by means of time-series analysis, to assess the presence of significant narrow-band periodic components. Thomson's multitaper method (MTM; Thomson, 1982) was used to identify the main spectral components, and spectra were tested against a robust red noise model (Mann and Lees, 1996) to constrain the significance of the interpreted features (Fig. 6). Each time series, being obtained from different locations, can be considered as an independent replication and can be used to assess the stability of significant spectral peaks across the three series.

Some spectral peaks rising above the 99% confidence interval (CI) are common in all three series (Fig. 6). A peak around 1 cycle/m is significant in all three series (L, C, and R) and is one of the more stable spectral features found in the three signals. A narrow frequency component with a period of ~1.94 m (1.9 in L, 1.98 in C, 1.93 in R) is also consistently present in all time series. A higher-frequency couplet at ~1.2 cycle/m (0.8 m in a period) is common in both the C and R series, although slightly shifted in frequency. Finally, a component with periods of 1.22 m in L, 1.33 m in C, and 1.18 m in R is also significant. Cycles longer than ~5 m are less consistent among the three series, although a component with a period around 7–8 m (well above the CI) is present in C, and it just reaches the 90% CI in L and is absent in R.

[2]Source code can be found at https://github.com/luca-penasa/vombat.

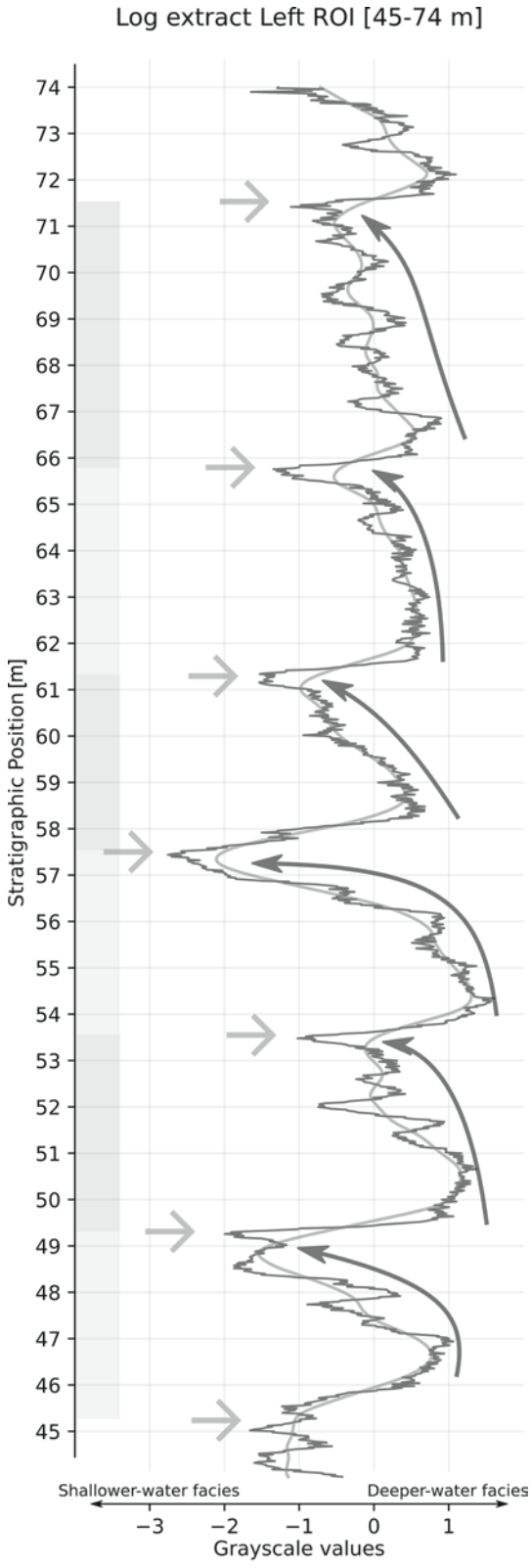

Figure 5. Extract of grayscale log illustrating the expression of the asymmetric pattern due to the shallowing-upward peritidal cycle of the Calcare Massiccio. ROI—region of interest.

Cycles with periods shorter than 0.6 m (1.5 cycle/m) were not considered because they could not be easily linked to real features (e.g., bundles of layers) in the succession.

Figure 7A shows just the confidence levels reached by the spectral power at varying frequencies. Peaks that are close to 100% CI are those that more likely identify a real periodic component. Averaging the CI between the three series, the frequencies of the spectral peaks that appear to be consistently present in all three time series can be highlighted and correspond to periods of 3.74, 1.94, 1.36, 1.23, and 1.01 m (Fig. 7B).

Preliminary Cyclostratigraphy for the Calcare Massiccio at Gola della Rossa

Because no radiometric ages for Calcare Massiccio are available, and biostratigraphic constraints are poor, we applied average spectral misfit (ASM; Meyers and Sageman, 2007) to assess the likelihood of orbital forcing on the deposition of the Calcare Massiccio. ASM is provided in the Astrochron R package (Meyers, 2014) and enables iterative testing for the presence of orbital cycles in sedimentation within a plausible range of sedimentation rates. It includes a formal statistical test for rejecting the null hypothesis of no orbital signal based on Monte Carlo simulations.

The spectral components to be tested (in the space domain) are selected from the signal's MTM spectrum using the following criteria: they are above a defined "robust" confidence level, and they pass an *F*-test (Thomson, 1982). These spatial frequencies, expressed in cycle/m, can be transformed into true time periodicities by assuming a sedimentation rate (*SR*) for the series under investigation:

$$f_{\text{time}} = f_{\text{space}} \times SR. \quad (1)$$

The ASM method makes it possible to test a large number of possible sedimentation rates: for each sedimentation rate, the frequencies in the space domain are transformed to the time domain and then compared to a series of "target" frequencies expressed in the time domain. This comparison is quantified by the ASM scalar, which is computed for each tested sedimentation rate. Lower ASM values correspond to better fit, while larger values correspond to poor fit with the target frequencies. To quantify the likelihood of obtaining spectral components in a specific arrangement by pure chance, the ASM method performs a Monte Carlo simulation, which enables the user to compute a CI for the observed ASM values.

For this analysis, we used a composite time series generated by merging different parts extracted from the L and C time series. Although it was a composite time series, it does represent the best continuous stratigraphic log of the Calcare Massiccio at the Gola della Rossa quarry that we could produce. The 16 frequencies from the MTM spectrum of the composite series that were above the 85% CI and passed the *F*-test were used for ASM (Fig. 8). As target frequencies, we used those corresponding to long

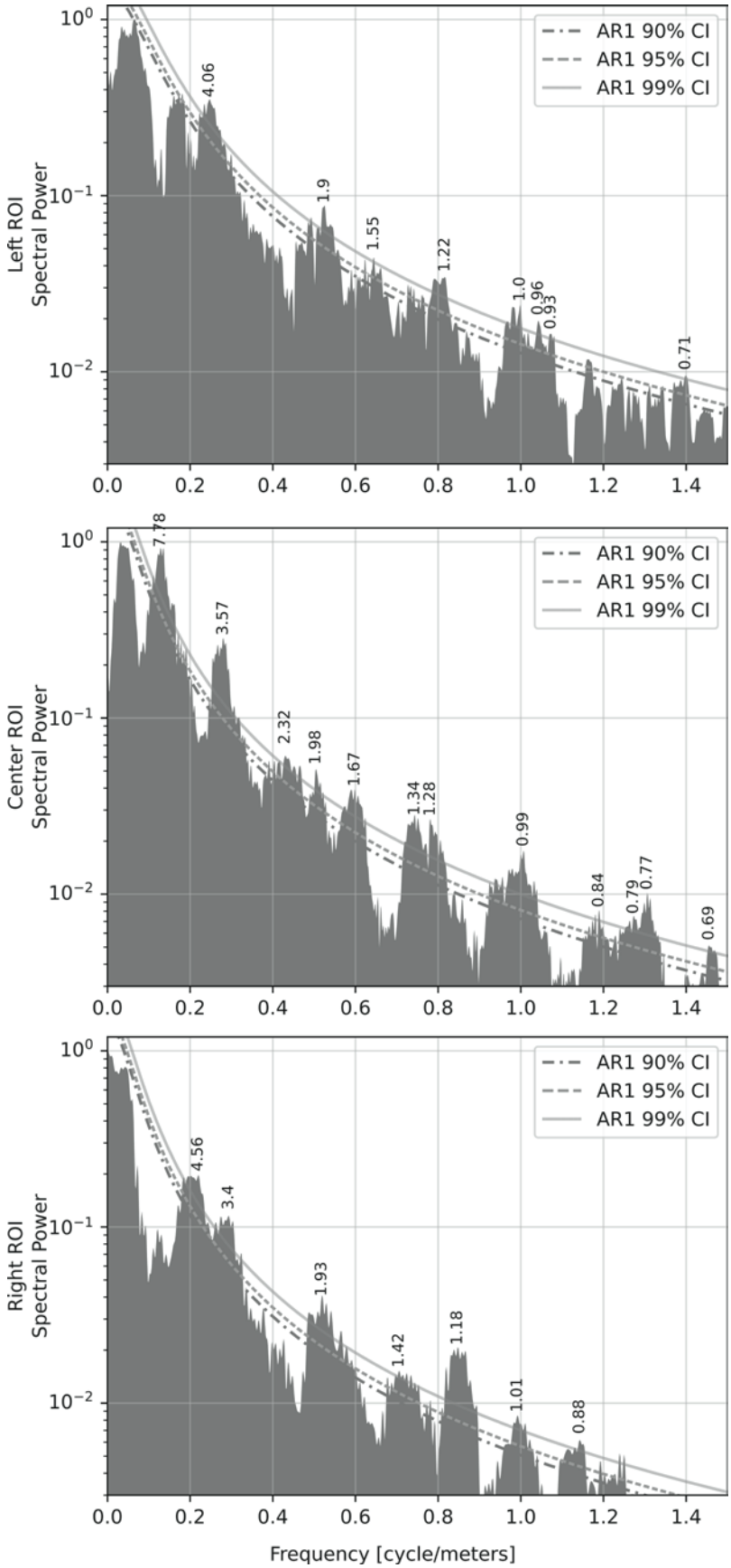

Figure 6. Power spectra of the three time series (L, C, and R) and significant peaks as determined from an autoregressive noise model of first order (AR1), computed with the mtmML96 routine of the Astrochron package (Meyers, 2014). ROI—region of interest; CI—confidence interval.

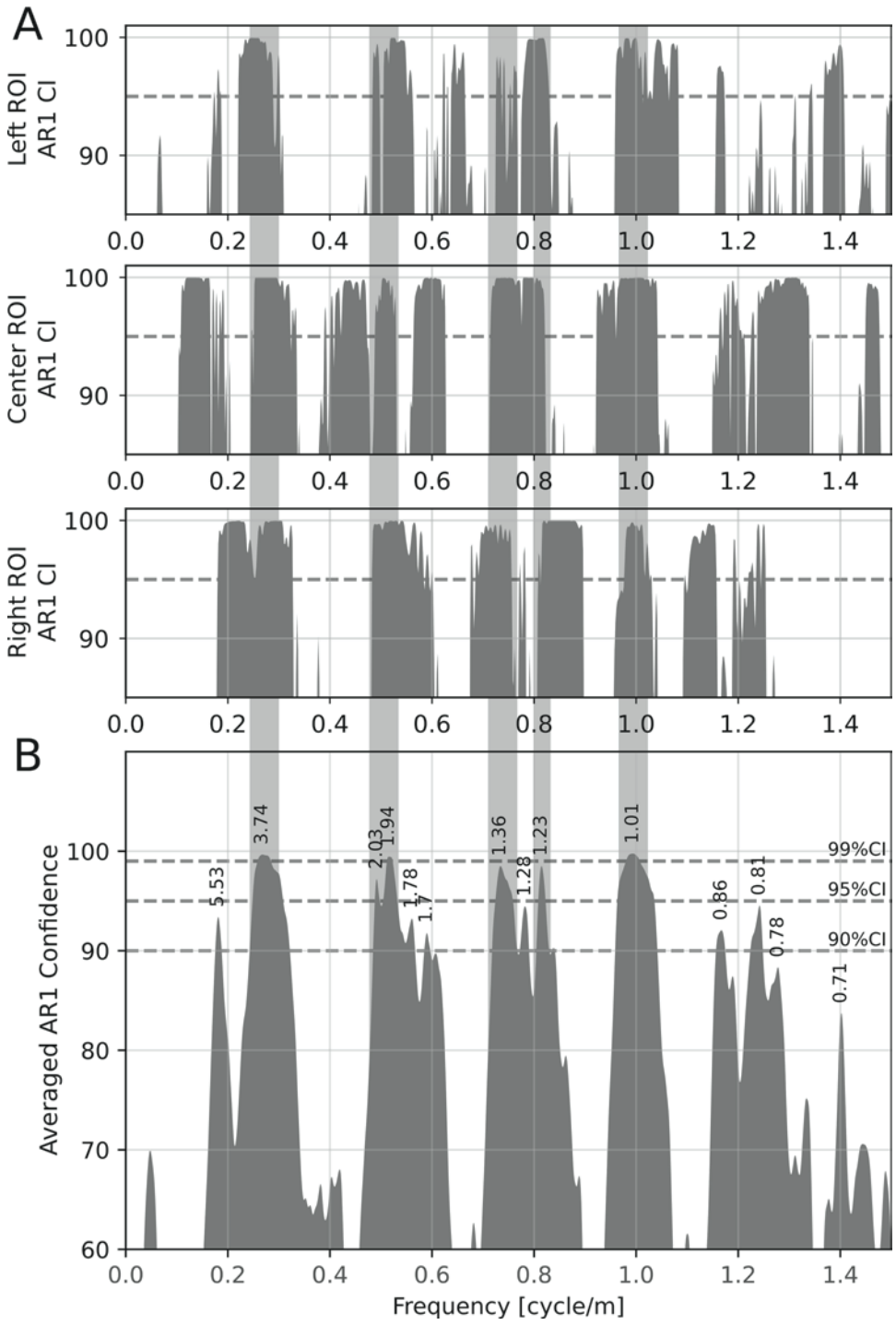

Figure 7. (A) Statistical significance (under the autoregressive noise model of first order [AR1], i.e., red noise, hypothesis) of the spectral features for the three independent time series obtained from the L, C, and R regions of interest (ROIs). Highlighted are spectral peaks that are more consistently shared by all three time series. (B) Average significance (average of plots of panel A) helps to illustrate the common frequencies that are also statistically significant in the three data sets. CI—confidence interval.

eccentricity, short eccentricity, obliquity, and precession predicted by the La2004 astronomical solution (Laskar et al., 2004). Various sedimentation rates from 0 to 150 m/m.y. were tested with ASM. Two sedimentation rates, at 50 m/m.y. and 90 m/m.y., were found to be statistically significant. For these rates, the chance of obtaining the measured ASM value by randomly distributed frequencies was well below 1% (Fig. 9).

DISCUSSION

Photologs of cores proved to be a good source of cyclostratigraphic data (Grippo et al., 2004), while portable spectrophotometers were also employed in the field for the same purpose (e.g., Batenburg et al., 2014). The rationale of these approaches is that changes in color of the rocks can be related to changes in the

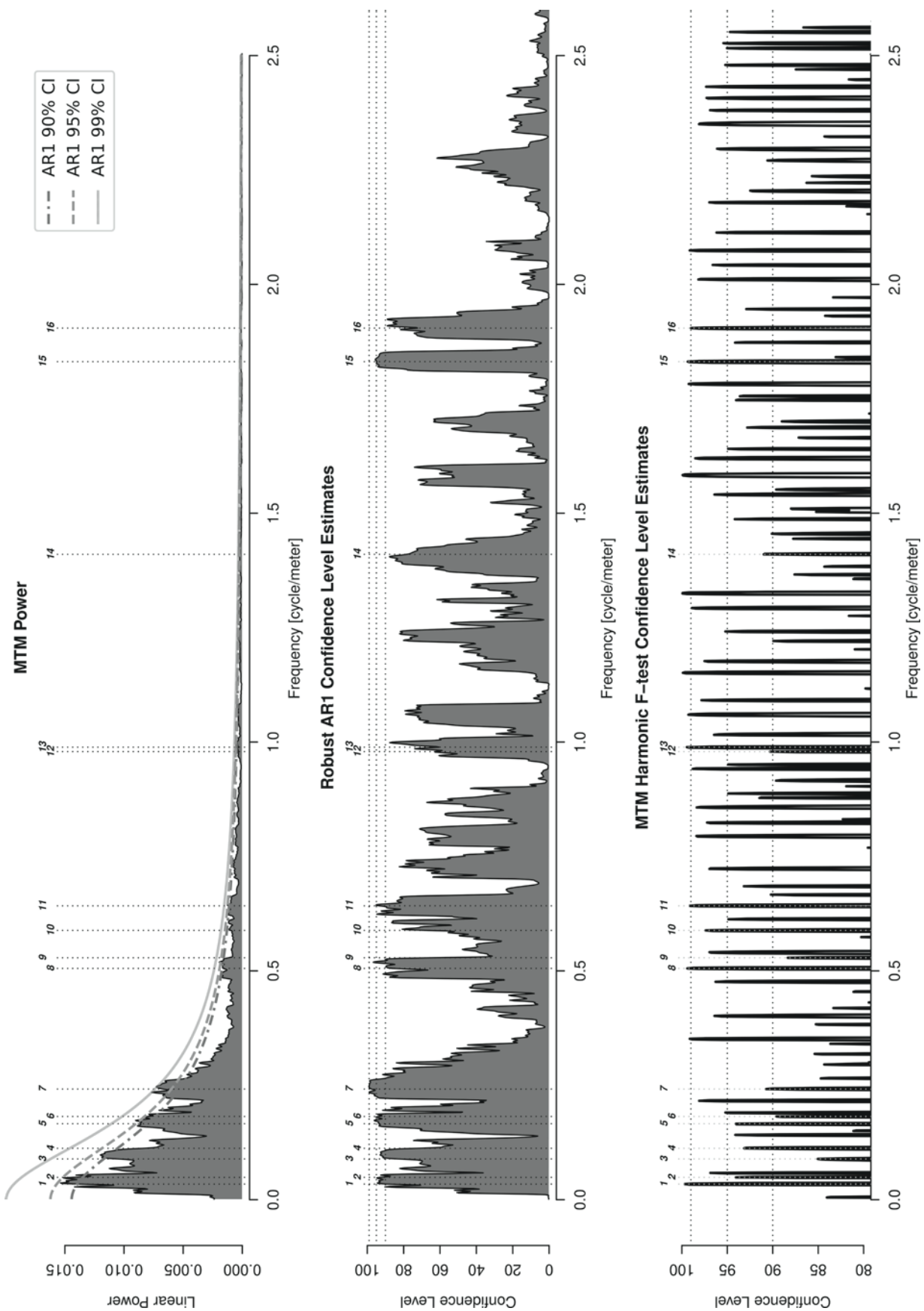

Figure 8. Thomson 4π spectrum for the composite time series obtained by merging different pieces of the C and L series (using the multitaper method [MTM]; Thomson, 1982). Identified spectral components, which passed both the red-noise and the *F*-test, are labeled with numbers and were used to assess the possible presence of an orbital forcing within the data set, by using the average spectral misfit method. AR1—autoregressive noise model of first order; CI—confidence interval.

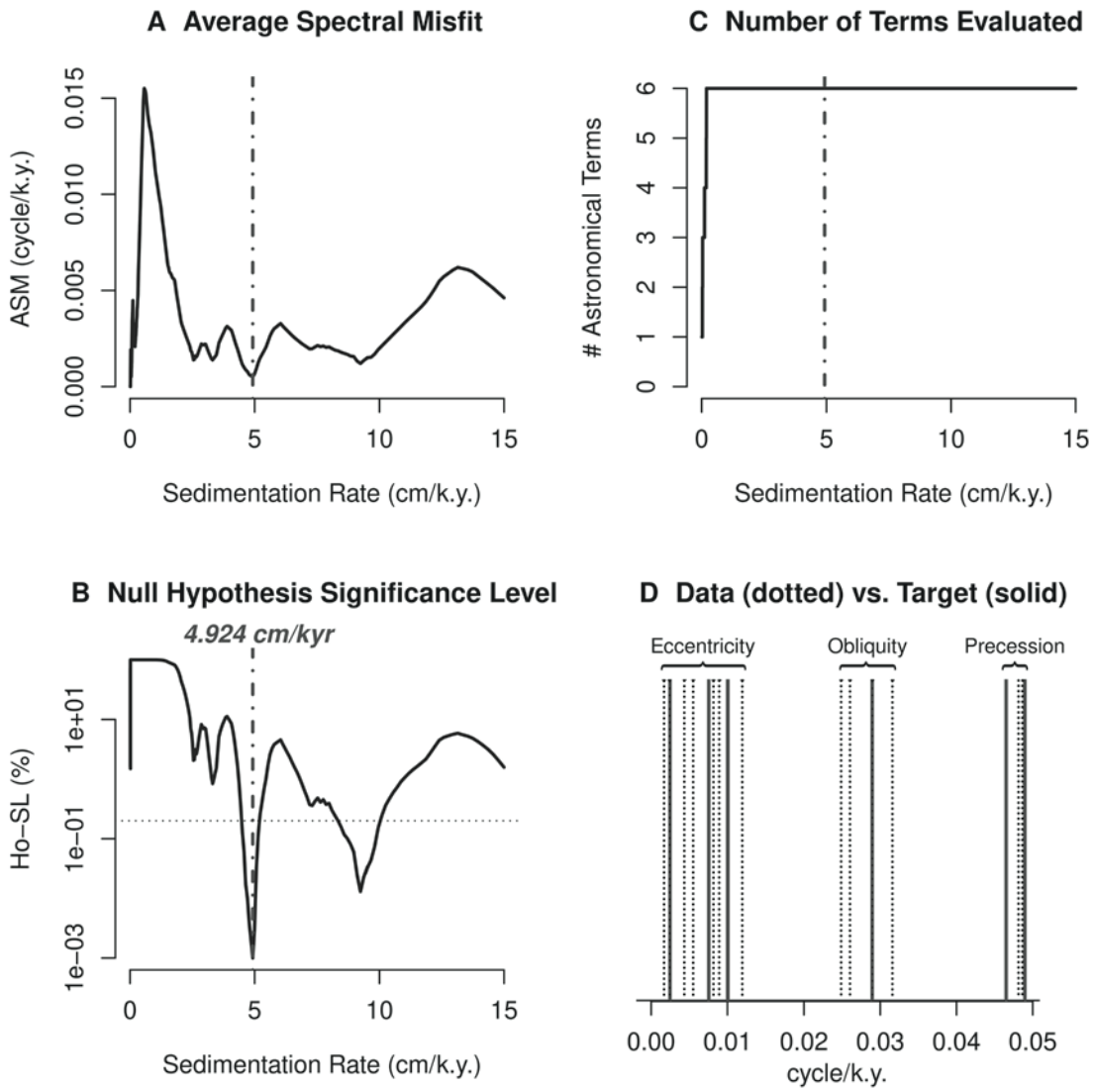

Figure 9. Results of the average spectral misfit (ASM). (A) ASM values at varying sedimentation rates; lower values mean a better fit to the expected Milankovitch frequencies, as computed by Laskar et al. (2004). (B) Significance level (SL) for the null hypothesis (H_0 = not having orbital influence in the data) at varying sedimentation rates: Two statistically significant minima are present at 50 m/m.y. and 90 m/m.y. (C) The number of astronomical terms in the target signal that are correctly matched to input ones. (D) Significant frequencies in the input signal expressed in the time domain given the sedimentation rate yielded by the ASM (dotted lines), plotted with the frequencies (in cycle/k.y.) of the target orbital terms (solid lines). Note that input frequencies form three groups that coincide with the main bands of the target orbital frequencies, i.e., the long to short eccentricity band (405–100 k.y.), the obliquity band (~30 k.y.), and the precession band (~20 k.y.).

depositional environments. Although in the case of the Calcare Massiccio, color variability is restricted to a palette ranging from dark to light gray–brownish, analysis of hand samples from the short accessible portion of the quarry indicated that supratidal facies are characterized by dark-gray colors while subtidal facies exhibit light-gray colors.

The grayscale series can be therefore used as a proxy of the main facies, and even if absolute grayscale values cannot be directly associated to specific facies, their relative variations reflect facies variability. For instance, the main shallowing-upward peritidal cycles that range in thickness between 4 and 5 m are nicely captured in the grayscale series (Fig. 5).

Obviously, imaging gives information about the surface of the rocks, and therefore it is highly sensitive to, for instance, weathering, humidity, and dust, which can influence the outcrop color. Therefore, the portions of the point cloud used for

generating the grayscale series were visually selected in the cleaner regions of the quarry wall. Despite this, some large-scale variations could still be due to changes in color due to weathering or humidity, but also due to variations in the lighting of the imaged surface. These changes are expected to affect large portions of the quarry wall (e.g., if the base of the outcrop is in shadow while the top is directly illuminated) and introduce low-frequency oscillations in the grayscale values (longer than tens of meters in period) along the series. A clear example is the R time series, where long-period variations in the grayscale values due to large-scale differences in the color of the outcrop are seen, while they do not occur in the same stratigraphic interval of the L and C series (Fig. 4).

The three logs were obtained from different portions of the quarry and can thus be considered to be independent realizations of the same stratigraphic log (although each has some missing portions, and they differ in extent). Hence, it is possible to perform a comparison of the spectral features present in three independently produced data sets: if a periodic signal is significant in one of the series, then it would be expected to be significant also in the others; otherwise, it might be the result of random fluctuations in the series. From the comparison of the three spectra (Figs. 6 and 7), we were indeed able to identify several narrow-band features that appear to be persistent in all the series, suggesting the presence of several common periodic components that can be associated to observable stratigraphic features.

Brandano et al. (2015) carried out facies-rank spectral analysis in a section located some 100 km SSW of the Gola della Rossa quarry and concluded that, although tectonics could not be completely disregarded as a potential driver, orbitally induced sea-level changes could be responsible for the formation of the Calcare Massiccio peritidal cycles, and this yielded a sedimentation rate of ~33 m/m.y.

Results of ASM applied on the Gola Della Rossa grayscale series obtained through photogrammetry in this work (Fig. 9) yielded 50 m/m.y. and 90 m/m.y. as the two sedimentation rates that better match the most significant spatial cyclicities found in the time series to the orbital periodicities predicted for the Early Jurassic by the La2004 orbital solution (Laskar et al., 2004). If the 50 m/m.y. option is preferred, cycles with thickness between 1.5 m and 2 m may be interpreted as corresponding to the obliquity cycle (~36 k.y.), cycles between 3 m and 5 m should correspond to the short eccentricity (~100 k.y.), while the 1 m component can be assigned to precession (around 20 k.y.). Such periodicities would imply that the main peritidal cycle (the one highlighted in Fig. 5) of the Calcare Massiccio is related to the short eccentricity. It is worth pointing out that high-precision calibration to short-period astronomical frequencies of the La2004 solution (Laskar et al., 2004) is limited by the instability of orbital dynamics for epochs prior to 60–50 Ma. Hence, what we present here should be considered as a preliminary assessment of whether the major periodicities recognizable in the Calcare Massiccio could display reciprocal ratios compatible with astronomical forcing. This is confirmed by the fact that the significant periodicities in the Calcare Massiccio of the Gola Della Rossa quarry, when the sedimentation rate yielded by ASM (50 m/m.y.) is considered, appear to match the main bands of the orbital frequencies (Fig. 9).

Variations in the sedimentation rates may have occurred during the deposition of the Calcare Massiccio at Gola Della Rossa. The Calcare Massiccio is referred to a time span of ~10 m.y. (comprising Hettangian and Sinemurian ages) that for a thickness of 700 m would suggest an average sedimentation rate around 70 m/m.y. (Petti et al., 2007). The results of ASM, with the two main most-likely sedimentation rates, indeed may be interpreted as evidence that significant variations in sedimentation rates might be present in the considered stratigraphic interval. Nevertheless, sedimentation rates identified by ASM are in the range of the average sedimentation rates of ~30 m/m.y. estimated for Tethyan Early Jurassic carbonate platforms (Bosence et al., 2009). Furthermore, a 50 m/m.y. sedimentation rate is roughly in agreement with the findings of Brandano et al. (2015) for the Calcare Massiccio in the Cornicolani Mountains (33 m/m.y.).

CONCLUSIONS

The results presented in this paper show the potential of photogrammetry in retrieving data suitable for cyclostratigraphic analysis of stratigraphic successions that would not be suitable for direct analysis because of their inaccessibility.

A complete 3-D photogrammetric model was obtained at the Gola della Rossa quarry, where the Early Jurassic carbonates of the Calcare Massiccio are exposed. The outcrop would have been otherwise inaccessible, but thanks to the 3-D model and the recorded RGB information, information was obtainable about the characteristics of the rocks. Direct facies analysis on an accessible portion of the quarry revealed that grayscale values obtained from the RGB colors can be used as a proxy for the facies variations in the Gola Della Rossa quarry. Hence, grayscale logs representing facies variations in the Calcare Massiccio were generated, and time-series analysis revealed the presence of statistically significant narrow-band periodic components, among which the one corresponding to the main peritidal cycle can be recognized. A composite grayscale series representative of the entire imaged stratigraphic interval was analyzed by means of the ASM method to test whether the observed cyclicities could be referred to orbital forcing. ASM yielded 50 m/m.y. as the sedimentation rate at which sedimentary periodicities observed in the Calcare Massiccio at Gola Della Rossa better fit orbital periods predicted for the Early Jurassic by the La2004 astronomical solution. Our results demonstrate that the periodicity of the Calcare Massiccio is indeed arranged in narrow spectral features displaying reciprocal ratios compatible with an astronomical forcing. A more detailed and robust cyclostratigraphic characterization of the Calcare Massiccio would require reference to age models based on independent methods such as biostratigraphy or radiometric dating. However, these results, which are in good agreement with independent cyclostratigraphic interpretations (Brandano et al., 2015),

confirm that orbital forcing might have been a major driver in the deposition of the shallow-water carbonates of the Calcare Massiccio, thus reinforcing the evidence that the recording of astronomical signals in carbonate platforms is, under favorable conditions, indeed possible (Kemp et al., 2016).

ACKNOWLEDGMENTS

We wish to thank Linda Hinnov (George Mason University, Fairfax, Virginia) for the fruitful discussions about time-series processing and analysis, Daniel Girardeau-Montaut and the other developers of the CloudCompare community, for their efforts in maintaining and enhancing the software, and Luc Girod for the help provided with MicMac. Raffaele Poidomani of the Gola Della Rossa Quarry Company granted access to the quarries. The comments of Walter Alvarez (University of California, Berkeley, California) and an anonymous reviewer greatly helped in improving the quality of this work. The Association "Le Montagne di San Francesco" provided logistical support during fieldwork.

REFERENCES CITED

Batenburg, S.J., Gale, A.S., Sprovieri, M., Hilgen, F.J., Thibault, N., Boussaha, M., and Orue-Etxebarria, X., 2014, An astronomical time scale for the Maastrichtian based on the Zumaia and Sopelana sections (Basque country, northern Spain): Journal of the Geological Society, v. 171, p. 165–180, https://doi.org/10.1144/jgs2013-015.

Bice, D.M., and Stewart, K.G., 1985, Ancient erosional grooves on exhumed bypass margins of carbonate platforms: Examples from the Apennines: Geology, v. 13, no. 8, 565–568, https://doi.org/10.1130/0091-7613(1985)13<565:AEGOEB>2.0.CO;2.

Bosence, D., Procter, E., Aurell, M., Bel Kahla, A., Boudagher-Fadel, M., Casaglia, F., Cirilli, S., Mehdie, M., Nieto, L., Rey, J., Scherreiks, R., Soussi, M., and Waltham, D., 2009, A dominant tectonic signal in high-frequency, peritidal carbonate cycles? A regional analysis of Liassic platforms from western Tethys: Journal of Sedimentary Research, v. 79, p. 389–415, https://doi.org/10.2110/jsr.2009.038.

Brandano, M., Corda, L., Tomassetti, L., and Testa, D., 2015, On the peritidal cycles and their diagenetic evolution in the Lower Jurassic carbonates of the Calcare Massiccio Formation (Central Apennines): Geologica Carpathica, v. 66, p. 33, https://doi.org/10.1515/geoca-2015-0033.

Buckley, S.J., Howell, J.A., Enge, H.D., and Kurz, T.H., 2008, Terrestrial laser scanning in geology: Data acquisition, processing and accuracy considerations: Journal of the Geological Society [London], v. 165, p. 625–638, https://doi.org/10.1144/0016-76492007-100.

Buckley, S.J., Kurz, T.H., Howell, J.A., and Schneider, D., 2013, Terrestrial LiDAR and hyperspectral data fusion products for geological outcrop analysis: Computers & Geosciences, v. 54, p. 249–258, https://doi.org/10.1016/j.cageo.2013.01.018.

Burton, D., Dunlap, D.B., Wood, L.J., and Flaig, P.P., 2011, Lidar intensity as a remote sensor of rock properties: Journal of Sedimentary Research, v. 81, p. 339–347, https://doi.org/10.2110/jsr.2011.31.

Carminati, E., Corda, L., Mariotti, G., Scifoni, A., and Trippetta, F., 2013, Mesozoic syn- and postrifting evolution of the Central Apennines, Italy: The role of Triassic evaporites: The Journal of Geology, v. 121, p. 327–354, https://doi.org/10.1086/670730.

Colacicchi, R., Passeri, L., and Pialli, G., 1975, Evidences of tidal environment deposition in the Calcare Massiccio Formation (Central Apennines—Lower Lias), *in* Ginsburg, R.N., ed., Tidal Deposits: Berlin, Springer, p. 345–353, https://doi.org/10.1007/978-3-642-88494-8_39.

Coltorti, M., and Bosellini, A., 1980, Sedimentazione e tettonica nel Giurassico della dorsale marchigiana: Studi Geologici Camerti, v. 6, p. 13–21.

Cozzi, A., Hinnov, L.A., and Hardie, L.A., 2005, Orbitally forced Lofer cycles in the Dachstein Limestone of the Julian Alps (northeastern Italy): Geology, v. 33, p. 789–792, https://doi.org/10.1130/G21578.1.

Dupraz, C., Reid, R.P., Braissant, O., Decho, A.W., Norman, R.S., and Visscher, P.T., 2009, Processes of carbonate precipitation in modern microbial mats: Earth-Science Reviews, v. 96, p. 141–162, https://doi.org/10.1016/j.earscirev.2008.10.005.

Fischer, A.G., 1964, The Lofer cyclothems of the Alpine Triassic: Kansas Geological Survey Bulletin, v. 169, p. 107–149.

Franceschi, M., Teza, G., Preto, N., Pesci, A., Galgaro, A., and Girardi, S., 2009, Application of terrestrial laser scanner to cyclostratigraphy: ISPRS International Journal of Photogrammetry and Remote Sensing, v. 64, p. 522–528, https://doi.org/10.1016/j.isprsjprs.2009.03.003.

Franceschi, M., Preto, N., Hinnov, L.A., Huang, C., and Rusciadelli, G., 2011, Terrestrial laser scanner imaging reveals astronomical forcing in the Early Cretaceous of the Tethys realm: Earth and Planetary Science Letters, v. 305, p. 359–370, https://doi.org/10.1016/j.epsl.2011.03.017.

Franceschi, M., Penasa, L., Coccioni, R., Gattacceca, J., Smit, J., Cascella, A., Mariani, S., and Montanari, A., 2015, Terrestrial laser scanner imaging for the cyclostratigraphy and astronomical tuning of the Ypresian–Lutetian pelagic section of Smirra (Umbria–Marche Basin, Italy): Palaeogeography, Palaeoclimatology, Palaeoecology, v. 440, p. 33–46, https://doi.org/10.1016/j.palaeo.2015.08.027.

Girardeau-Montaut, D., 2014, Cloudcompare: A 3D Point Cloud and Mesh Processing Free Software: Paris, EDF R&D and Telecom ParisTech, http://cloudcompare.org (accessed May 2019).

Grippo, A., Fischer, A.G., Hinnov, L.A., Herbert, T.D., and Premoli Silva, I., 2004, Cyclostratigraphy and chronology of the Albian Stage (Piobbico core, Italy), *in* D'Argenio, B., and Zühlke, R., eds., Cyclostratigraphy: Approaches and Case Histories: Society for Sedimentary Geology (SEPM) Special Publication 81, p. 57–81, https://doi.org/10.2110/pec.04.81.0057.

Hodgetts, D., 2013, Laser scanning and digital outcrop geology in the petroleum industry: A review: Marine and Petroleum Geology, v. 46, p. 335–354, https://doi.org/10.1016/j.marpetgeo.2013.02.014.

Kemp, D.B., Van Manen, S.M., Pollitt, D.A., and Burgess, P.M., 2016, Investigating the preservation of orbital forcing in peritidal carbonates: Sedimentology, v. 63, no. 6, p. 1701–1718, https://doi.org/10.1111/sed.12282.

Kern, A.K., Harzhauser, M., Soliman, A., Piller, W.E., and Mandic, O., 2013, High-resolution analysis of Upper Miocene lake deposits: Evidence for the influence of Gleissberg-band solar forcing: Palaeogeography, Palaeoclimatology, Palaeoecology, v. 370, p. 167–183, https://doi.org/10.1016/j.palaeo.2012.12.005.

Kirillova, N.P., and Sileva, T.M., 2017, Colorimetric analysis of soils using digital cameras: Moscow University Soil Science Bulletin, v. 72, p. 13–20, https://doi.org/10.3103/S0147687417010045.

Kondrashov, D., and Ghil, M., 2006, Spatio-temporal filling of missing points in geophysical data sets: Nonlinear Processes in Geophysics, v. 13, p. 151–159, https://doi.org/10.5194/npg-13-151-2006.

Kurz, T.H., Buckley, S.J., and Howell, J.A., 2012, Close range hyperspectral imaging integrated with terrestrial LiDAR scanning applied to rock characterization at centimeter scale: The International Archives of the Photogrammetry, Remote Sensing and Spatial Information Sciences, v. 39, p. 417–422, https://doi.org/10.5194/isprsarchives-XXXIX-B5-417-2012.

Laskar, J., Robutel, P., Joutel, F., Gastineau, M., Correia, A.C.M., and Levrard, B., 2004, A long-term numerical solution for the insolation quantities of the Earth: Astronomy & Astrophysics, v. 428, p. 261–285, https://doi.org/10.1051/0004-6361:20041335.

Lugli, S., 2001, Timing of post-depositional events in the Burano Formation of the Secchia valley (Upper Triassic, Northern Apennines), clues from gypsum–anhydrite transitions and carbonate metasomatism: Sedimentary Geology, v. 140, p. 107–122, https://doi.org/10.1016/S0037-0738(00)00174-3.

Mann, M.E., and Lees, J.M., 1996, Robust estimation of background noise and signal detection in climatic time series: Climatic Change, v. 33, p. 409–445, https://doi.org/10.1007/BF00142586.

Marino, M., and Santantonio, M., 2010, Understanding the geological record of carbonate platform drowning across rifted Tethyan margins: Examples from the Lower Jurassic of the Apennines and Sicily (Italy): Sedimentary Geology, v. 225, p. 116–137, https://doi.org/10.1016/j.sedgeo.2010.02.002.

Martinis, B., and Pieri, P., 1964, Alcune notizie sulla formazione evaporitica del Triasssico superiore nell'Italia centrale e meridionale: Memorie Società Geologica Italiana, v. 4, p. 649–678.

McCaffrey, K.J.W., Jones, R.R., Holdsworth, R.E., Wilson, R.W., Clegg, P., Imber, J., Holliman, N., and Trinks, I., 2005, Unlocking the spatial dimension: Digital technologies and the future of geoscience fieldwork: Journal of the Geological Society, v. 162, p. 927–938, https://doi.org/10.1144/0016-764905-017.

Meyers, S.R., 2014, Astrochron: An R Package for Astrochronology: https://cran.r-project.org/package=astrochron (accessed May 2019).

Meyers, S.R., and Sageman, B.B., 2007, Quantification of deep-time orbital forcing by average spectral misfit: American Journal of Science, v. 307, p. 773–792, https://doi.org/10.2475/05.2007.01.

Penasa, L., Franceschi, M., Preto, N., Teza, G., and Polito, V., 2014, Integration of intensity textures and local geometry descriptors from terrestrial laser scanning to map chert in outcrops: ISPRS Journal of Photogrammetry and Remote Sensing, v. 93, p. 88–97, https://doi.org/10.1016/j.isprsjprs.2014.04.003.

Petti, M., Falorni, P., and Marino, M., 2007, Calcare Massiccio, *in* Carta Geologica d'Italia. Catalogo delle Formazioni-Unità Tradizionali (1): Rome, Italy, Quaderni del Servizio Geologico d'Italia, serie VI, volume 7(VII), scale 1:50,000.

Rupnik, E., Daakir, M., and Pierrot Deseilligny, M., 2017, MicMac—A free, open-source solution for photogrammetry: Open Geospatial Data, Software, and Standards, v. 2, p. 14, https://doi.org/10.1186/s40965-017-0027-2.

Santantonio, M., Galluzzo, F., and Gill, G., 1996, Anatomy and palaeobathymetry of a Jurassic pelagic carbonate platform/basin system, Rossa Mts, Central Apennines (Italy): Geological implications: Palaeopelagos, v. 6, p. 123–169.

Schwarzacher, W., 1993, Cyclostratigraphy and the Milankovitch Theory: Amsterdam, Elsevier Science, Developments in Sedimentology 52, 224 p.

Thomson, D.J., 1982, Spectrum estimation and harmonic analysis: Proceedings of the Institute of Electrical and Electronics Engineers, v. 70, p. 1055–1096, https://doi.org/10.1109/PROC.1982.12433.

Trinks, I., Clegg, P., McCaffrey, K., Jones, R., Hobbs, R., Holdsworth, B., Holliman, N., Imber, J., Waggott, S., and Wilson, R., 2005, Mapping and analysing virtual outcrops: Visual Geosciences, v. 10, p. 13–19, https://doi.org/10.1007/s10069-005-0026-9.

Westoby, M.J., Brasington, J., Glasser, N.F., Hambrey, M.J., and Reynolds, J.M., 2012, 'Structure-from-motion' photogrammetry: A low-cost, effective tool for geoscience applications: Geomorphology, v. 179, p. 300–314, https://doi.org/10.1016/j.geomorph.2012.08.021.

Zeeden, C., Hilgen, F., Röhl, U., Seelos, K., and Lourens, L., 2015, Sediment color as a tool in cyclostratigraphy—A new application for improved data acquisition and correction from drill cores: Newsletters on Stratigraphy, v. 48, p. 277–285, https://doi.org/10.1127/nos/2015/0064.

Zeeden, C., Krauß, L., Kels, H., and Lehmkuhl, F., 2016, Digital image analysis of outcropping sediments: Comparison to photospectrometric data from Quaternary loess deposits at Şanoviţa (Romania) and Achenheim (France): Quaternary International, v. 429, p. 100–107, https://doi.org/10.1016/j.quaint.2016.02.047.

Zinßer, T., Schmidt, J., and Niemann, H., 2005, Point set registration with integrated scale estimation, in Eighth International Conference on Pattern Recognition and Image Processing, 18–20 May: Minsk, Belarus, Belarusian State University of Informatics and Radioelectronics, International Association for Pattern Recognition, p. 116–119.

Manuscript Accepted by the Society 27 February 2019
Manuscript Published Online 2 August 2019